ORIGINAL PAPER

Effect of Zr doping and Li_2O-$2B_2O_3$ layer on the structural electrochemical properties of $LiNi_{0.5}Co_{0.2}Mn_{0.3}O_2$ cathode material: experiments and first-principle calculations

Liubin Song[1] · Xinyu Li[1] · Zhongliang Xiao[1] · Lingjun Li[2] · Zhong Cao[1] · Huali Zhu[2]

Abstract

In order to enhance the electrochemical performance of $LiNi_{0.5}Co_{0.2}Mn_{0.3}O_2$ (NCM), an in situ doping with zirconium (Zr) by wet grind-solid state method then coating with Li_2O-$2B_2O_3$ (LBO) by crystal phase selection method is successfully developed. At the same time, based on the density functional theory (DFT) with the generalized gradient approximation (GGA), use of the first-principle calculation method theoretically proved the experimental results. The XRD results of experimental and the calculated both revealed the lattice parameters become larger after Zr doped. The thickness of the LBO layer uniformly deposited on the surface of the Zr-doped sample is 5 nm, which can scavenge and neutralize HF erosion. Particularly, the Zr-doped and LBO-coated NCM sample exhibited excellent cycling performance with 90.5% capacity retention after 100 cycles at 1 C, which are apparently higher than 76.97% of NCM. The initial discharge capacity of double optimized sample was 170.4 mAh g^{-1} at 1 C which is higher than 157.1 mAh g^{-1} of NCM. Zr and LBO layers can effectively reduce the energy of the system and the band gap. Obtained results were consistent with the experimental results. Therefore, co-modification method plays an import role to optimize the material from the structure to the surface and hence greatly improved the battery performance.

Keywords $LiNi_{0.5}Co_{0.2}Mn_{0.3}O_2$ · Co-modification · Electrochemical performance · Lithium-ion battery · First-principle calculations

Introduction

Energy shortages and environmental hazards are regarded as the most important issues by all countries in the world. Lithium-ion batteries are getting an upsurge of interest as a source of green energy due to their high energy density, simple working mechanism, and environmentally friendly properties. The ternary cathode material $LiNi_xCo_yMn_zO_2$ possesses an advantage over the traditional cathode materials ($LiCoO_2$, $LiNiO_2$, and $LiMnO_2$) due to ternary synergistic effect [1, 2]. Among them, $LiNi_{0.5}Co_{0.2}Mn_{0.3}O_2$ (NCM) material is considered to be relatively more stable with higher discharge capacity, hence regarded as the ideal material for electric vehicles' power source. However, during the charging and discharging of the material, due to the close proximity of Ni^+ and Li^+ radius resulting in cation mixing, lattice defects caused by collapse of the layered structure, and corrosion caused by the electrolyte solution, the cycle performance, consistency, and safety are affected [3–7].

In the experimental section, bulk doping and surface coating are considered as two major effective methods of modification. Doped atom such as Al [8], Sb [9], Zr [10], and Na [11] has radius similar to Li^+, which caused charge compensation mechanism in order to solve the structural collapse problem. The coating layer separated the cathode material and the electrolyte by certain conductive material such as Al_2O_3 [12], Li_2ZrO_3 [13], and $LiAlO_2$ [14] to relieve the side reactions.

✉ Zhongliang Xiao
csustslb@csust.edu.cn

1 Hunan Provincial Key Laboratory of Materials Protection for Electric Power and Transportation, School of Chemistry and Biological Engineering, Changsha University of Science and Technology, Changsha 410004, Hunan, China

2 School of Materials Science and Engineering, Changsha University of Science and Technology, Changsha 410004, Hunan, China

In the theoretical data section, understanding of the effect of doping and coating in NCM is still far from clear. Computational science plays a vital role in the design of advanced cathode materials. It successfully predicted and interpreted the properties and behaviors of Al and Mg doping on the degradation in $LiNi_{0.8}Co_{0.1}Mn_{0.1}$ [15], and studied electrolyte interfacial reaction of $LiCoO_2$ [16]. Zr has the ability to enhance the metal strength of the material, modify the distance of lithium ion and metal layer, and hence aimed to improve electronic and lithium ion conduction. LBO is considered as a very ideal coating material because of its properties such as glass network structure and relatively low viscosity. The oxygen vacancies formed facilitated the insertion and extraction of Li^+. The mobility of ion and its sub-lattice structure made Li^+ to have high diffusion capacity. Li_2O-$2B_2O_3$ has two crystal forms at different calcining temperatures; the tri-polyboron formed at low temperature is prone to absorb water and affects the performance of the material. Lithium tetraborate formed at a high temperature causes volume expansion, resulting in increased ionic conductivity. Therefore, temperature is a key factor in the preparation process [17, 18]. Further study of material properties and thermal behavior at the molecular level by first-principle calculations which based on density functional theory (DFT) predicted the material properties and explain the optimization principles. These information can further verify the veracity and repeatability of the experimental conclusions to promote rational design [19].

This paper combined experimental methods and a computational approach to investigate the effect of doping with zirconium (Zr) by wet grind-solid state method and coating the surface with Li_2O-$2B_2O_3$ (LBO) by crystal phase selection method in NCM. In the doping process, the grinding was performed in a wet environment, which greatly reduced the material cracks caused by excessive mechanical stress before the segment burning. At the same time, the crystal shape of the material is selected by controlling the temperature. The effects of Zr doping and LBO coating amount on electrochemical performance of samples by co-modification were also investigated. At the same time, the first principles of double-optimized material calculations based on band and state densities further demonstrate the effectiveness of the optimization.

Experimental

Sample preparation

Layered $LiNi_{0.5}Co_{0.2}Mn_{0.3}O_2$ (NCM) was obtained via wet grind-solid state method. Using LiOH and commercial precursor $Ni_{0.5}Co_{0.2}Mn_{0.3}(OH)_2$ grinded in alcohol at the molar ratio of 1:1.05. Calcined at 500 °C for 5 h and then at 900 °C for 15 h. Zr doped sample $LiNi_{0.5}Co_{0.2}Mn_{0.3}O_2)_{0.98}Zr_{0.02}O_2$ (NCMZ) via the same way using $Ni_{0.5}Co_{0.2}Mn_{0.3}(OH)_2$, LiOH, and zirconia at the molar ratio of 1:1.05:0.02. In preparation, Li_2O-$2B_2O_3$-$(LiNi_{0.5}Co_{0.2}Mn_{0.3}O_2)_{0.98}Zr_{0.02}O_2$ (LBO-NCMZ) was synthesized by crystal phase selection method. It was obtained by LiOH and H_3BO_3 as the starting materials were initially dissolved in CH_3OH at the molar ratio of 1:2 then NCMZ power synchronously added to solution. Continuous slowly stirring was performed at 80 °C until the solution was evaporated. Finally, the powder was calcined at 500 °C for 10 h. The LBO coating procedure and the mechanism for Li-ion conduction are shown in Fig. 1. And the detailed chemical mechanisms of this reaction were presented as (1) as follows [20, 21].

Fig. 1 The LBO glass coating procedure and the mechanism of Li-ion conduction in the LBO coating layer

$$2LiOH + 4H_3BO_3 \rightarrow Li_2O-2B_2O_3 + 7H_2O \qquad (1)$$
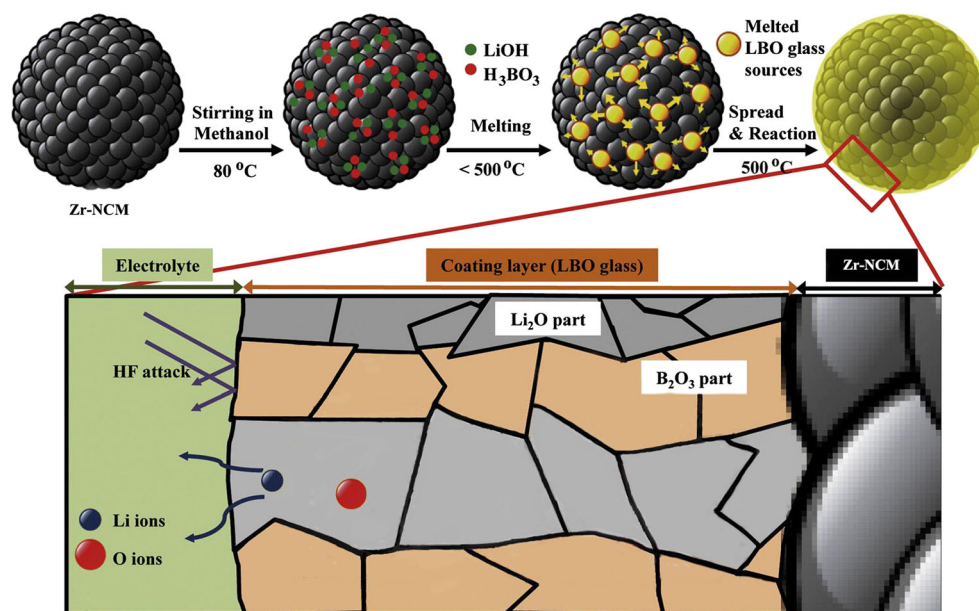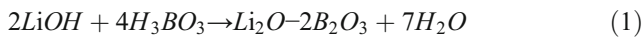
Characterization techniques

The crystal structures of the products were confirmed by X-ray powder diffraction (XRD) using Cu-Kα radiation at scanning rate of 5° min^{-1} under the incidence angle range of 10°–80°. The morphology of the particles were measured by scanning electron microscope (SEM) with an accelerating voltage of 20 kV equipped with an energy-dispersive spectrometer (EDS) and high-resolution transmission electron microscope (HRTEM).

Electrochemical measurement

The cathode electrodes were fabricated by pasting a slurry composed of the as-prepared active materials, polyvinylidene difluoride (PVDF), and carbon black at a ratio of 8:1:1. Then, the mixture was dispersed in *N*-methyl-2-pyrrolidinone (NMP) and the slurry was coated onto aluminum foil. The electrochemical behaviors of the prepared cathode materials were investigated using a CR2025 coin-type cells. Cyclic voltammetry (CV) measurements were performed in a range of 2.5–4.8 V at a 0.1 mV s^{-1}. Electrochemical impedance spectroscopy (EIS) was also carried out after different numbers with a frequency range from 0.01 Hz to 100 kHz.

First-principle calculation

First, find the structural parameters of NCM, NCMZ, and LBO-NCMZ using FindIt software. The PW91 (Perdew Wang (1991)) method in the spin-polarized generalized gradient approximation (GGA) method was used. Energy, band structure, and density of states with NCM, NCMZ, and LBO-NCMZ were calculated by CASTEP module. Density of states with energy tolerance selection is 1.0×10^{-5} eV.

Results and discussion

X-ray diffraction

Figure 2 shows the XRD patterns of NCM, NCMZ, and LBO-NCMZ, without impurities or secondary diffraction peaks. The phase of the products after optimizing the conditions was found basically the same as that of NCM; the spatial point group R-3m peak position and the lattice constant were also not changed. All of them were observed similar to that of α-NaFeO$_2$ layered structure [22]. Remarkably, the (108)/(110) and (006)/(102) peaks were clearly split, indicating that all the samples were crystallized well. The (003) peaks were shifted to
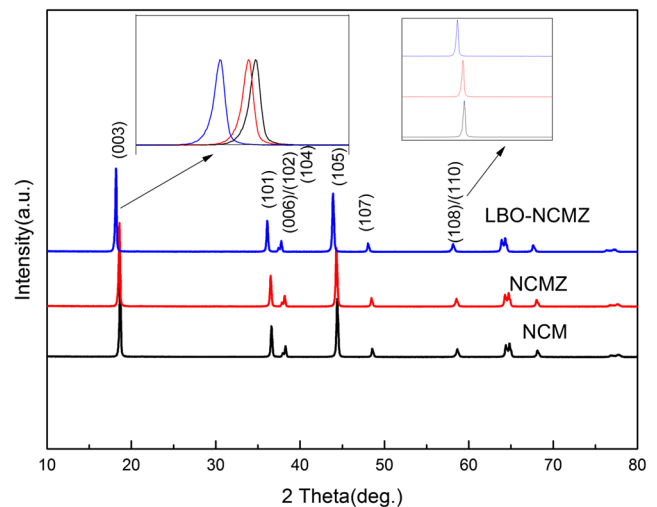

Fig. 2 XRD patterns of NCM, NCMZ, and LBO-NCMZ

lower degree for NCMZ and LBO-NCMZ samples. Table 1 shows the greater *c/a* value of NCMZ and LBO-NCMZ as compared to that of NCM. Drawn in the cation mixing degree was reduced and the inter-planar spacing was found larger. Zr was successfully intercalated into the crystal structure. Little change in the coated sample demonstrated that coating on the surface of cathode material was done with amorphous LBO glass only.

Microstructural characterization

SEM images of NCM, NCMZ, and LBO-NCMZ are shown in Fig. 3a–f. Figure 3a–c shows that the doping and coating did not affect the basic spherical morphology of the NCM. Figure 3d, e clearly demonstrates the larger size of NCMZ than NCM. The particle size was observed to be 10–15 μm. Figure 3f shows the LBO-NCMZ spherical surface coating being slightly rough as compared to that of NCMZ and LBO-NCMZ, indicating that the LBO coating behavior was effective. After cycles, the globular morphology of the NCM will be found destroyed and the structure collapsed utterly. However, the spherical morphology of LBO-NCMZ could be isolated from the cathode material and electrolyte, eased HF corrosion of the cathode material.

Figure 4c–e shows EDS spectra of LBO-NCMZ were performed to check the uniformity of Ni, Co, and Mn on LBO-NCMZ. Elemental dot mapping shown in Fig. 4b, f proved the

Table 1 Lattice constants of NCM, NCMZ, and LBO-NCMZ

Samples	*a* (Å)	*c* (Å)	*c/a*
NCM	2.871	14.222	4.954
NCMZ	2.878	14.235	4.946
LBO-NCMZ	2.867	14.240	4.967
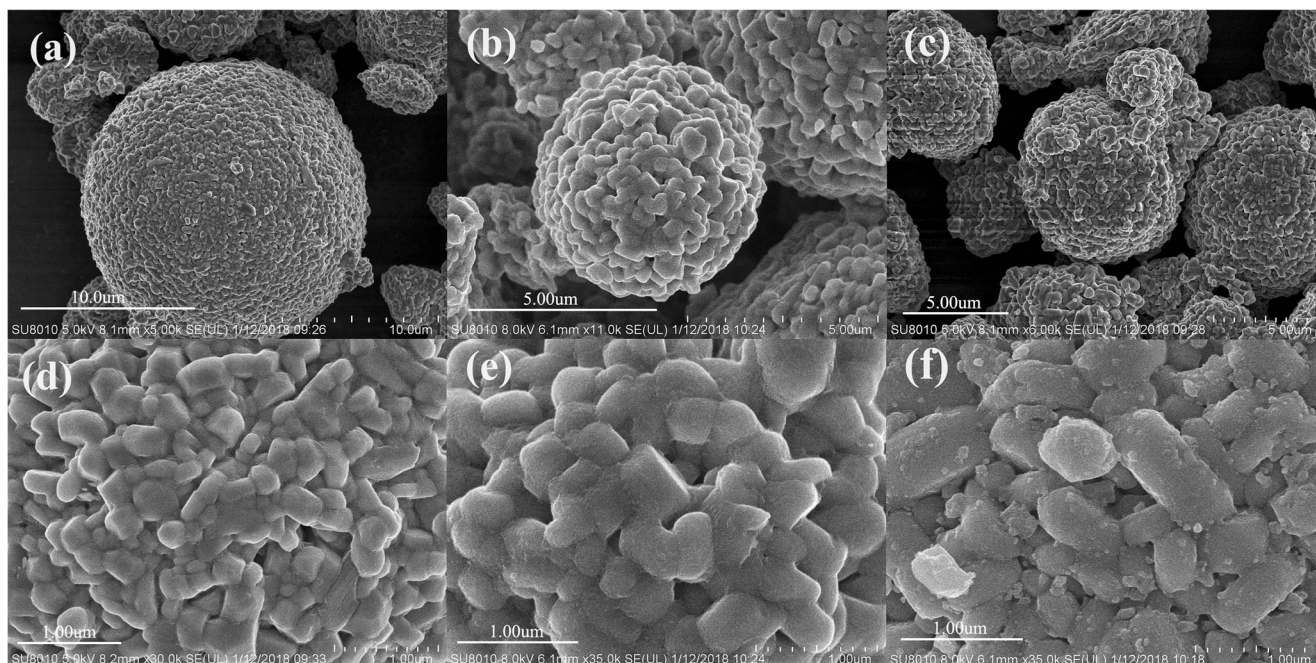
Fig. 3 SEM images of NCM (**a**, **d**), NCMZ (**b**, **e**), and LBO-NCMZ (**c**, **f**)

homogeneous distribution of Zr and B elements in LBO-NCMZ sample. Further, it demonstrated that doping and coating were effective method to improve material properties.

Figure 5a–f illustrates the TEM images of NCM, NCMZ, and LBO-NCMZ. Obviously, TEM images further proved the existence of LBO coating. Figure 5a–c represents that the surface of positive electrode was smooth without coating. As can be seen in Fig. 5d–f, the coated material with the obvious thickness of about 5 nm was present on the surface of NCMZ. This layer acted as a conductive agent and a binder that inhibited the change in volume from layered structure to

spinel structure during charge and discharge. Hence, this method resulted in improving the material stability.

Electrochemical performance

Figure 6 represents the first charge-discharge curves of NCM, NCMZ, and LBO-NCMZ at a current of 1 C. The capacity of each sample was found to be 157.1, 174.4, and 170.4 mAh g^{-1}. NCMZ values were noticed to be higher than that of NCM, as Zr doping was carried out to improve the ionic conductivity. LBO-NCMZ values
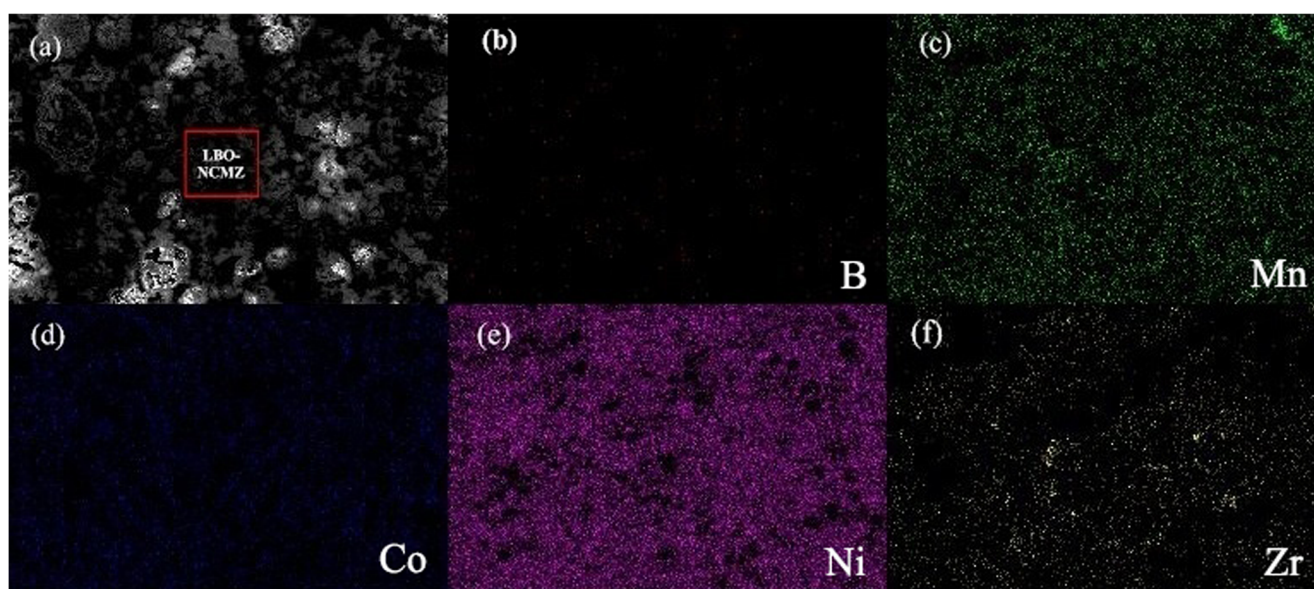

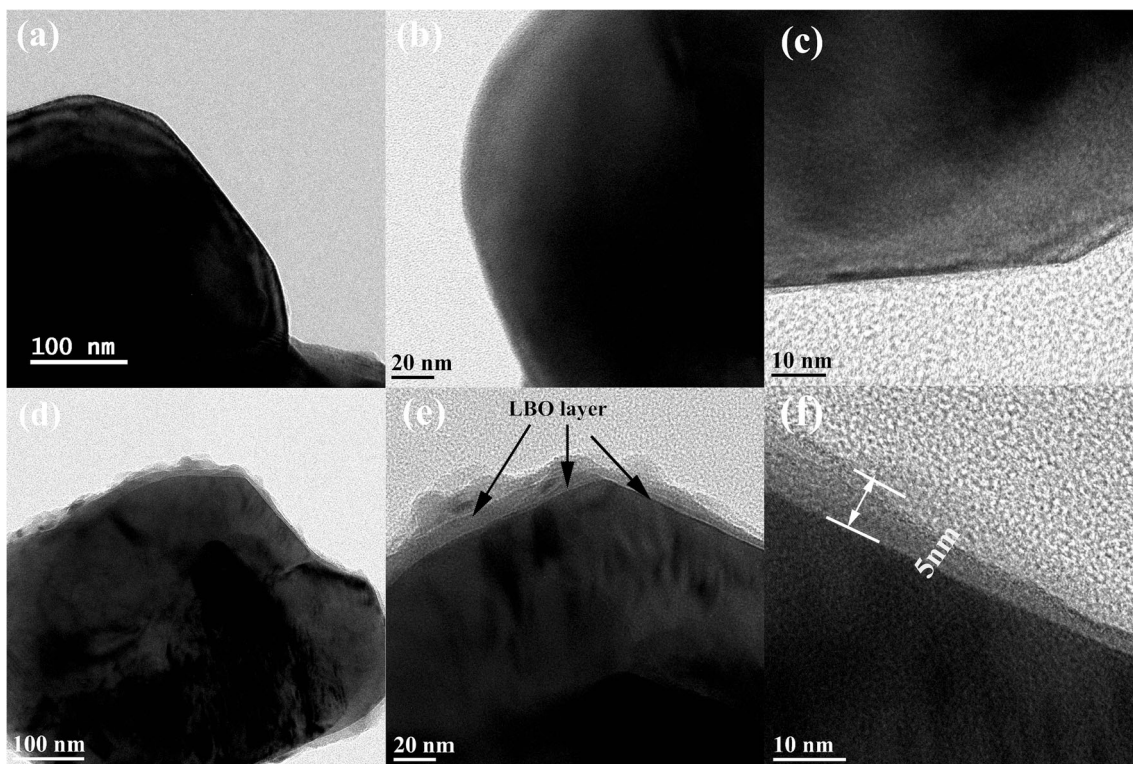Fig. 4 **a** SEM image of the LBO-NCMZ EDS mapping of **b** B, **c** Mn, **d** Co, **e** Ni, and **f** Zr

Fig. 5 TEM images of **a** NCM, **b** NCMZ, **c** LBO-NCMZ, **d** LBO-NCMZ 100 nm, **e** LBO-NCMZ 20 nm, and **f** LBO-NCMZ 10 nm

were slightly lower than that of NCM, as the layer was electrochemically inert within this voltage range and the coating somewhat impeded the conduction of ions, which was found consistent with the TEM results.

Figure 7a represents the discharge curves of NCM, NCMZ, and LBO-NCMZ after 100 cycles at 0.1 C, with a capacity of 148mAhg^{-1}, 152mAhg^{-1}, 167 mAh g^{-1} having capacity retention of 76.97%, 82.4%, and 90.5%. As reported in the literature, using LBO as a coating layer can also improve the electrochemical performance of other materials [23]. Though the

Fig. 6 Initial charge-discharge curves of NCM, NCMZ, and LBO-NCMZ at 1 C

LBO-NCMZ samples delivered lower initial discharge capacities due to electrochemically inert layer, LBO glass was observed having good ionic conductivity and exerted positive effect on the cycling performance of the cathode material. Insufficient coating amount was still eroded by the electrolyte to form NiO, accompanied by oxygen loss and transition metal that was dissolved. Excessive amount of coating impeded the ion migration as reported in the literature.

The excellent rate property was also a remarkable advantage of the LBO-NCMZ that can be observed in Fig. 7b. NCM, NCMZ, and LBO-NCMZ electrodes were measured at different rates (0.1, 0.2, 1, and 2 C). At low rate of 0.1 C, NCM was compared with NCMZ and LBO-NCMZ having composite discharge capacity in close proximity. The discharge capacity of LBO-NCMZ sample was found to be 165.5 mAh g^{-1} which was higher than 159 mAh g^{-1} as observed for NCM at 2 C. Other material studies also indicate the larger the discharge rate and the greater the current, the more irreversible polarization of the electrode material occurred [24]. Co-modification eases the damage to the electrode material structure and morphology.
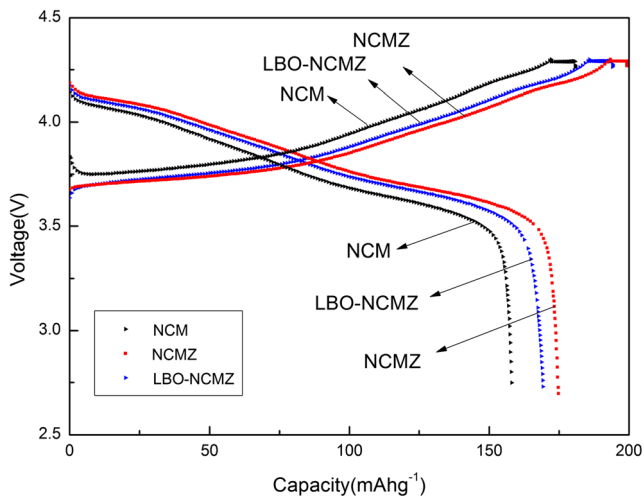
Cyclic voltammograms and electrochemical impedance spectroscopy

Figure 8a–d shows the cyclic voltammograms of NCM, NCMZ, and LBO-NCMZ. All curves shown were found similar in shape, indicating that the doping and coating did not
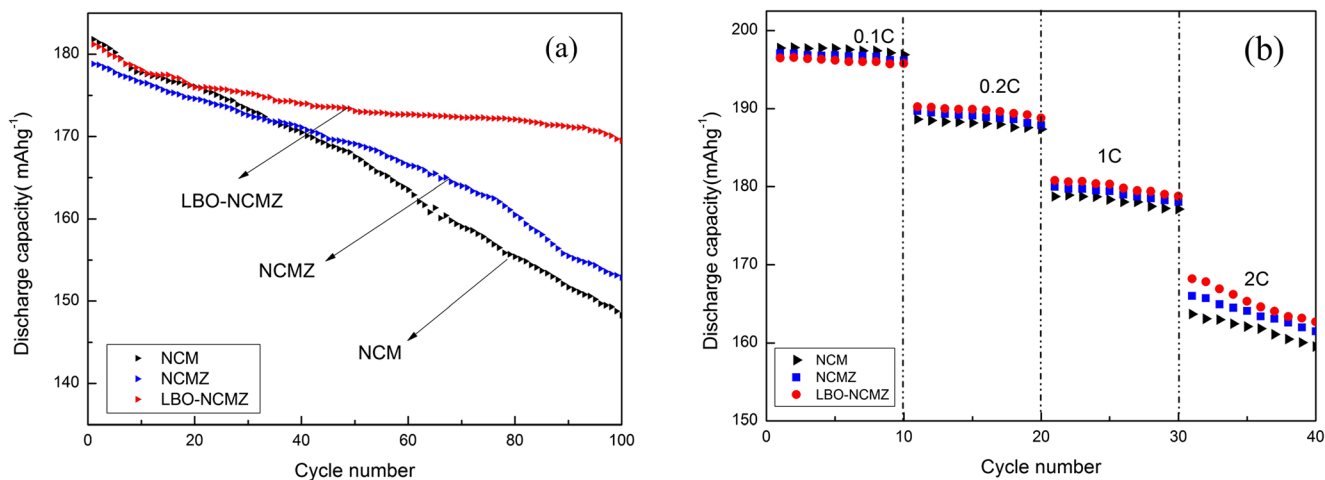
Fig. 7 **a** Cyclic performance of NCM, NCMZ, and LBO-NCMZ at 0.1 C. **b** Rate capability of NCM, NCMZ, and LBO-NCMZ at 1 C

affect the primary structure of NCM. Figure 8a shows that in the first cycle, the oxidation peak of NCM was noticed to be 4.366 V, while the reduction peak was 3.977 V. Figure 8b shows that the oxidation peak of NCMZ was found as 4.359 V, while the reduction peak was 4.025 V. Figure 8c shows that the oxidation peak of LBO-NCMZ was found as 3.968 V, while the reduction peak was 3.651 V. It clearly demonstrated that the irreversible polarization was smaller during charging and discharging and, hence, more conducive to the ion extraction and embedding. Figure 8d shows that
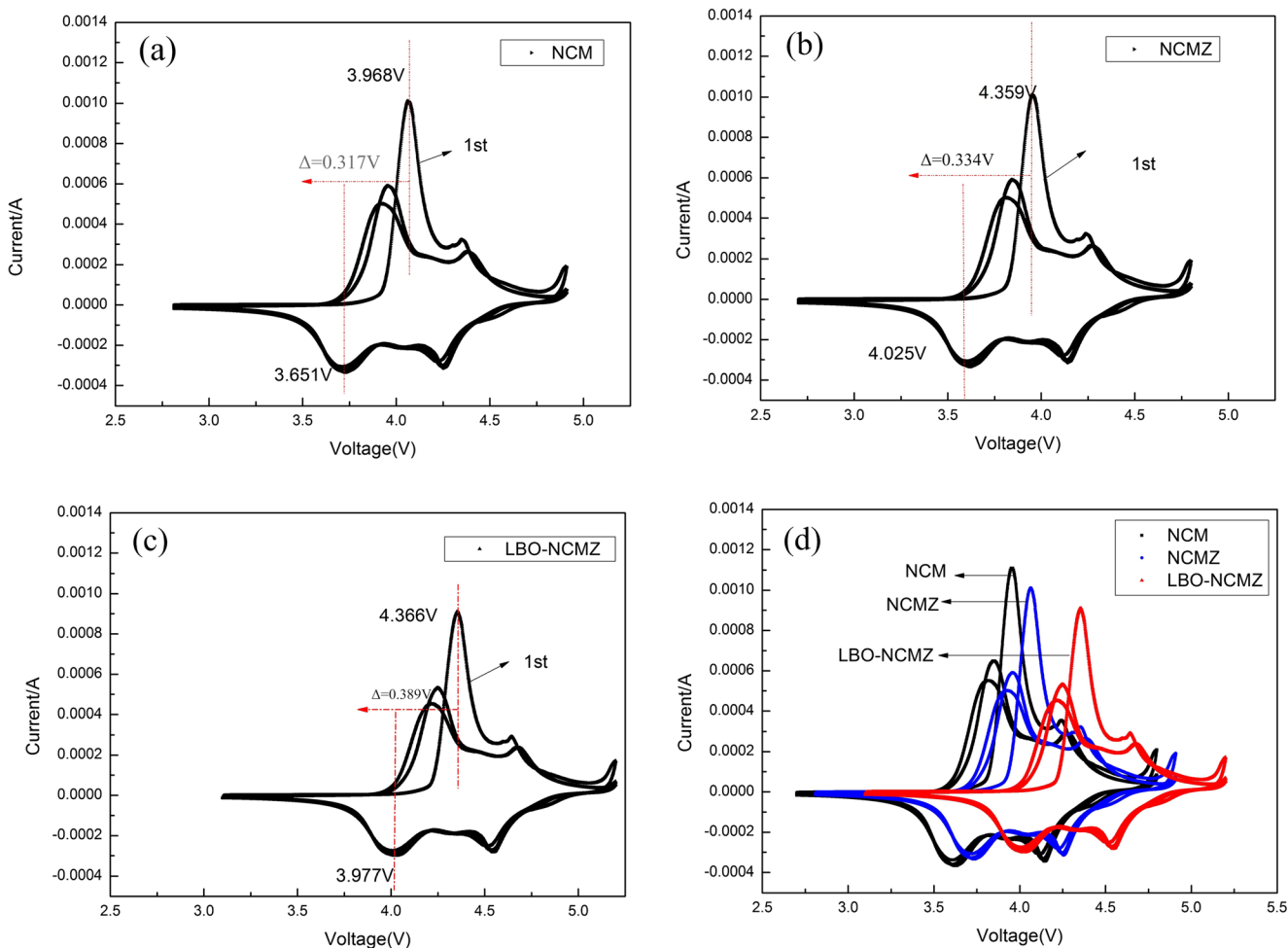

Fig. 8 Cyclic voltammograms of **a** NCM, **b** NCMZ, and **c** LBO-NCMZ. **d** Sample comparison chart
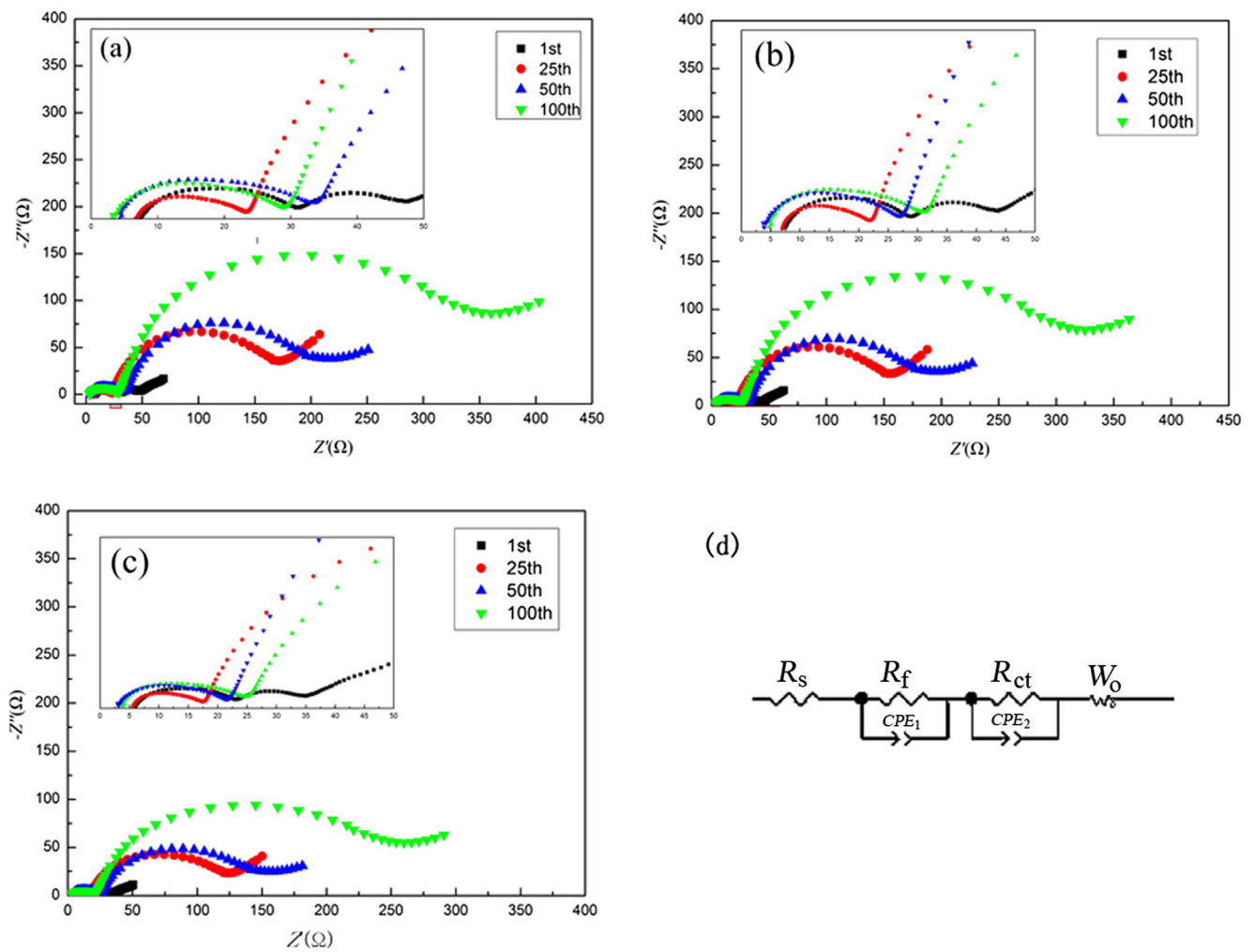
Fig. 9 a NCM, b LBO-NCMZ, and c LBO-NCMZ electrodes at the charge state of 4.6 V after the 1st and 50th cycles. d Nyquist plots of samples

after coating, the oxidation peak and reduction peak of the area formed were smaller, which signified that the material would have better cycling performance after coating. This is similar to the results of other optimization materials [25].

Figure 9a–c represents the EIS measurements of NCM, NCMZ, and LBO-NCMZ samples after the 1st, 25th, 50th, and 100th cycles. The intercept at the Z_{real}-axis in high frequency refers to uncompensated ohmic resistance

(R_s), which includes electric contact resistance, electrolyte solution resistance, and ion conductive resistance. The semicircle later emerged from high to medium frequency represented the charge transfer resistance (R_{ct}) between the electrode and electrolyte, a sloping line at low frequency which corresponded to the diffusion of lithium ions in the solid electrode (Z_w) [26, 27]. In general, low-frequency tail characteristic of the chemical diffusion process was found similar for the first cycle of each cell, but

Table 2 Impedance parameters fitted for the NCM, NCMZ, and LBO-NCMZ from equivalent circuits at 1 C conditions after different cycles

Cycles	NCM		NCMZ		LBO-NCMZ	
	R_f/Ω	R_{ct}/Ω	R_f/Ω	R_{ct}/Ω	R_f/Ω	R_{ct}/Ω
1st	23.1	92.0	21.5	15.1	21.1	19.8
25th	20.2	192.0	24.7	97.5	29.2	102.4
50th	18.0	374.3	25.8	162.9	14.4	154.5
100th	13.3	529.5	26.3	308.9	18.6	248.5

Table 3 Cell parameters and Fermi energies of NCM, NCMZ, and LBO-NCMZ

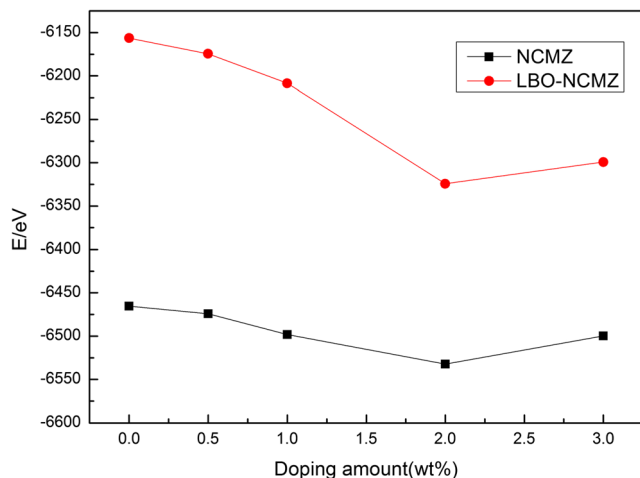| Samples	Cell parameter		Volume (Å)	Band gap (eV)
	A (Å)	C (Å)		
NCM	2.850	15.015	105.643	0.985
NCMZ	2.908	14.890	109.109	0.751
LBO-NCMZ	2.905	14.868	108.725	0.702

Fig. 10 Minimum energies of NCMZ and LBO-NCMZ with different doping amounts and coating amounts

the difference in the number of cycles was significant. The R_s value of NCMZ tends to be more stable than NCM as the number of cycles increased, and the R_s value of LBO-NCMZ was found below the R_s value of NCM. R_{ct} was increased on increasing the number of cycles as shown in Table 2. Figure 9d shows the Nyquist plots of samples. NCM value of R_{ct} was increased from the original value of 13.3 to 529.5 Ω after 100 cycles, while the R_{ct} value of LBO-NCMZ was increased from initial value of 19.8 to 248.5 Ω. These findings indicated that the application of Zr doping and LBO glass coating was an excellent strategy for suppressing the formation of SEI layer, suppressing the structure distortion, and facilitating the Li$^+$ migration at the surface of cathode.

First-principle calculations

Table 3 shows the optimized structural parameters of NCM, NCMZ, and LBO-NCMZ after first-principle calculations; it can be seen that the calculated unit cell parameters of each material and the experimental data have undergone minor changes. This acceptable change was due to experimental errors. Calculations showed that the c/a values of the unit cell increased and the volume increased 4.14%. This was similar to the experimental results of experiments as Table 1 shows the feasibility of the calculation method.

It was known from Fig. 10 the minimum energy curves of NCMZ and LBO-NCMZ with different doping and coating amounts (0.5, 1, 2, and 3 wt%). The energy of the system decreases first and then increases with increasing doping and coating amount. The transition metal with a large doping radius could cause a slight change in the crystal lattice, thereby reducing cation mixing, and the layer can mitigate surface corrosion and promote lattice stability. When the doping amount and the coating amount are 2 wt%, the energy of the system was the lowest and the performance was the most stable. This was consistent with the experimental results. Zr doping can reduce the energy gap, so that the energy of electrons to transition from the conduction band to the valence band decreases, and the position of the entire energy band moved in the low-energy direction. LBO coating can ease the occurrence of side reactions and reduce the energy loss during work.

Figure 11a–f presents the structure and density of states of NCM, NCMZ, and LBO-NCMZ near the Fermi level. From the band gap width in Fig. 11a–c, the doped and
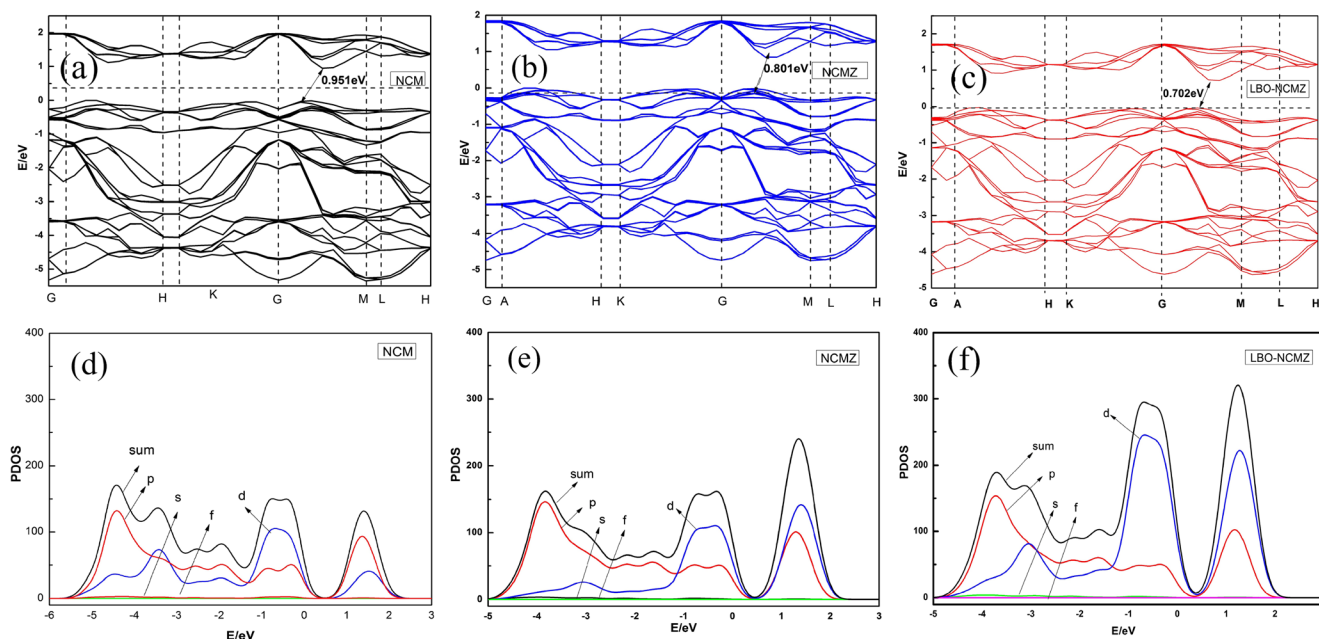

Fig. 11 Energy band and density of state of NCM (**a**, **d**), NCMZ (**b**, **e**), and LBO-NCMZ (**c**, **f**)

coated materials still belong to the semiconductor. After the completed doping optimization, the energy level difference between the valence band and the conduction band was reduced from 0.951 to 0.801 eV. When double optimization was performed, the energy difference between the conduction band and the valence band was the smallest, and the band gap reached 0.702 eV, making the electronic transition easier to occur, thereby increasing the conductivity of the material. It can be seen from the sum line that the energy density of the material was mainly determined by the electrons of the p and d orbitals. The electronic contributions of the s and f orbital orbits were small and can be neglected [28]. The calculation results showed that the theoretical results of the double modification method can be basically consistent with the experimental results.

Conclusions

The structural stability and electrochemical performance of $LiNi_{0.5}Co_{0.2}Mn_{0.3}O_2$ cathode materials were strengthened after Zr doping and LBO coating. First-principle calculations were performed on the double-modified material using calculation software. The experimental results and calculation results of XRD showed that the co-modification did not affect the NCM layered structure and improved material structure stability. TEM images clearly confirmed that the 5-nm LBO layer effectively separated the NCMZ. The capacity retention of LBO-NCMZ sample was noticed as 90.5% at 0.1 C after 100 cycles in 4.3 V, while that of NCMZ and NCM were 82.3 and 76.97%. R_{ct} value after 100 cycles was reduced from 529.5 to 248.5 Ω. Based on the analysis of the band structure and density of states, doping Zr and LBO layer can reduce the energy of the system while reducing the conductivity. It was found that the dual modification is better than single modification by characterizing two different kinds of optimized materials, which was proved by experimental and theoretical data.

References

1. Nitta N, Wu FX, Lee JT, Yushin G (2015) Li-ion battery materials: present and future. Materials Today 18(5):252–264
2. Liu YJ, Li XH, Guo HJ, Shen XQ (2010) Study on the improvement of cycling performance of manganese spinel battery. Chinese Battery Industry 4:003–004
3. Zheng HY, Qu QT, Zhu GB, Liu G, Battaglia VS, Zheng HH (2017) Quantitative characterization of the surface evolution for $LiNi_{0.5}Co_{0.2}Mn_{0.3}O_2$ graphite cell during long-term cycling. ACS Appl Mater Interfaces 9(14):12445–12452
4. Chen XL, Lu WZ, Chen C, Xue MZ (2018) Improved electrochemical performance of $LiNi_{0.5}Co_{0.2}Mn_{0.3}O_2$ cathode with different carbon additives for lithium-ion batteries. Int. J. Electrochem. Sci 13:296–304
5. Noh M, Cho J (2013) Optimized synthetic conditions of $LiNi_{0.5}Co_{0.2}Mn_{0.3}O_2$ cathode materials for high rate lithium batteries via co-precipitation method. J Electrochem Soc 160(1): 105–111
6. Meng K, Wang ZX, Guo HJ, Wang JX (2017) A compact process to prepare $LiNi_{0.8}Co_{0.1}Mn_{0.1}O_2$ cathode material from nickel-copper sulfide ore. Hydrometallurgy 174:1–9
7. Wang JX, Liu ZM, Yan GC, Li HK, Peng WJ, Li XH, Song LB, Shin K (2016) Improving the electrochemical performance of lithium vanadium fluorophosphate cathode material: focus on interfacial stability. J Power Sources 329:553–557
8. Dixit M, Markovsky B, Aurbach D, Major DT (2017) Unraveling the effects of Al doping on the electrochemical properties of $LiNi_{0.5}Co_{0.2}Mn_{0.3}O_2$ using first principles. J Electrochem Soc 164(1):6359–6365
9. He XS, Du CY, Shen B, Chen C, Xu X, Wang YG, Zuo PG, Ma YL, Cheng XQ, Yin GP (2017) Electronically conductive Sb-doped SnO_2 nanoparticles coated $LiNi_{0.8}Co_{0.15}Al_{0.05}O_2$ cathode material with enhanced electrochemical properties for Li-ion batteries. Electrochim Acta 236:273–279
10. Wang D, Li XH, Wang ZX, Guo HJ, Xu Y, Fan YL, Ru JJ (2016) Role of zirconium dopant on the structure and high voltage electrochemical performances of $LiNi_{0.5}Co_{0.2}Mn_{0.3}O_2$ cathode materials for lithium ion batteries. Electrochim Acta 188:48–56
11. Wang RH, Xiao SH, Li XH, Wang JX, Guo HJ, Zhong FX (2013) Structural and electrochemical performance of Na-doped $Li_3V_2(PO_4)_3$/C cathode materials for lithium-ion batteries via rheological phase reaction. J Alloys Compd 575:268–272
12. Dong MX, Wang ZX, Li HK, Guo HJ, Li XH, Shih K, Wang JX (2017) Metallurgy inspired formation of homogeneous Al_2O_3 coating layer to improve the electrochemical properties of $LiNi_{0.8}Co_{0.1}Mn_{0.1}O_2$ cathode material. ACS Sustainable Chem Engineering 5(11):10199–10205
13. Wu PH, Wang ZG, Liu SJ, Zhang L, Zhang Y (2015) Fabrication of Li^+ conductive Li_2ZrO_3-based shell encapsulated $LiNi_{0.5}Co_{0.2}Mn_{0.3}O_2$ microspheres as high rate and long life cathode materials for Li-ion batteries. ChemElectroChem 2(12):1921–1928
14. Li LJ, Chen ZY, Zhang QB, Xu M, Zhou X, Zhu HL, Zhang KL (2015) A hydrolysis-hydrothermal route for the synthesis of ultrathin $LiAlO_2$-inlaid $LiNi_{0.5}Co_{0.2}Mn_{0.3}O_2$ as a high-performance cathode material for lithium ion batteries. J Mater Chem A 3(2):894–904
15. Min K, Seo SW, Song YY, Lee HS, Cho EA (2017) First-principles study of the preventive effects of Al and Mg doping on the degradation in $LiNi_{0.8}Co_{0.1}Mn_{0.1}O_2$ cathode materials. Phys Chemistry Chem Phys 19(3):1762–1769
16. Tamura T, Kohyama M, Ogata S (2017) Combination of first-principles molecular dynamics and XANES simulations for $LiCoO_2$-electrolyte interfacial reactions in a lithium-ion battery. Phys Rev B 96(3):035107
17. Moe JK (1962) The crystal structure of lithium diborate, Li_2O-$2B_2O_3$. Acta Crystallogr 15(3):190–193
18. Aliev AE, Kholmanov IN, Khabibullaev PK (1999) Study of the thermoelectric power in amorphous and single crystalline lithium tetraborate Li_2O-$2B_2O_3$. Solid State Ionics 118(1–2):111–116
19. Yoon G, Kim DH, Park I, Chang D, Kim B, Lee B, Oh K, Kang K (2017) Using first-principles calculations for the advancement of materials for rechargeable batteries. Adv Funct Mater 27(40):1702887
20. Lim SN, Ahn W, Yeon SH, Park SB (2014) Enhanced elevated-temperature performance of $Li(Ni_{0.8}Co_{0.15}Al_{0.05})O_2$ electrodes coated with Li_2O-$2B_2O_3$ glass. Electrochim Acta 136:1–9

21. Choi SH, Kim JH, Ko YN, Hong YG, Kang YC (2012) Electrochemical properties of Li_2O-$2B_2O_3$ glass-modified $LiMn_2O_4$ powders prepared by spray pyrolysis process. J Power Sources 210:110–115

22. Li GY, Zhang ZJ, Wang R, Hung ZL, Zuo ZC, Zhou HH (2016) Effect of trace Al surface doping on the structure, surface chemistry and low temperature performance of $LiNi_{0.5}Co_{0.2}Mn_{0.3}O_2$ cathode. Electrochimica Acta 212:399–407

23. Chae JS, Yoon SB, Yoon WS, Kang YM, Park SM, Lee JW, Roh KC (2014) Enhanced high-temperature cycling of Li_2O–$2B_2O_3$-coated spinel-structured $LiNi_{0.5}Mn_{1.5}O_4$ cathode material for application to lithium-ion batteries. J Alloys Compd 601:217–222

24. Noh M, Cho J (2013) Optimized synthetic conditions of $LiNi_{0.5}Co_{0.2}Mn_{0.3}O_2$ cathode materials for high rate lithium batteries via co-precipitation method. J Electrochem Soc 160:105–111

25. Shi Y, Zhang MH, Qian DN, Meng YS (2016) Ultrathin Al_2O_3 coatings for improved cycling performance and thermal stability of $LiNi_{0.5}Co_{0.2}Mn_{0.3}O_2$ cathode material. Electrochimica Acta 203:154–161

26. Kim H, Kim MG, Jeong HY, Nam H, Cho J (2015) A new coating method for alleviating surface degradation of $LiNi_{0.6}Co_{0.2}Mn_{0.2}O_2$ cathode material: nanoscale surface treatment of primary particles. Nano Lett 15(3):2111–2119

27. Li J, Downie LE, Ma L, Qiu WD, Dahn JR (2015) Study of the failure mechanisms of $LiNi_{0.8}Mn_{0.1}Co_{0.1}O_2$ cathode material for lithium ion batteries. J Electrochem Soc 162(7):1401–1408

28. Hoang K (2017) First-principles theory of doping in layered oxide electrode materials. Phys.Rev.Mater 1(7):075403